

# Electronic Supporting Information

Linear-shaped  $\text{Ln}^{\text{III}}_4$  and  $\text{Ln}^{\text{III}}_6$  clusters constructed by polydentate Schiff base ligand and  $\beta$ -diketone co-ligand: structures, fluorescent properties, magnetic refrigeration and single-molecule magnet behavior

Wen-Min Wang,<sup>a,b</sup> Li-Yuan He,<sup>a</sup> Xin-Xin Wang,<sup>a</sup> Ying Shi,<sup>a</sup> Zhi-Lei Wu,<sup>\*b</sup> Jian-Zhong Cui<sup>\*b</sup>

## List of Contents

Experimental section.....	S2
Instrumentation.....	S2
Tables and Figure.....	S2–S8
Table S1. The $\text{Ln}^{\text{III}}$ geometry analysis by SHAPE 2.0 for clusters 6 and 7.....	S2
Fig. S1 The IR spectra of $\text{H}_2\text{L}$ ligand and clusters 1-10. ....	S3-S4
Fig. S2 The coordinate atom labels of central Dy(III) ions in cluster 6.....	S4
Fig. S3 The coordinate atom labels of central Er(III) ions in cluster 7.....	S4
Fig. S4 Coordination polyhedra for Er1, Er2 and Er3 ions observed in cluster 7.....	S5
Fig. S5 Coordination modes of $\text{H}_2\text{L}$ in 7.....	S5
Fig. S6 The coordinate atom labels of central Lu(III) ions in cluster 10.....	S5
Fig. S7 Coordination modes of $\text{H}_2\text{L}$ in cluster 10. ....	S5
Fig. S8 PXRD patterns for 1-10. ....	S6-S7
Fig. S9 The UV-vis spectra of clusters 1 -10 and the $\text{H}_3\text{L}$ ligand were performed at room temperature in ethanol solution. ....	S7
Fig. S10 Plots of $\chi_M^{-1}$ vs $T$ for 4. The solid line was generated from the best fit by the Curie-Weiss expression. ....	S7
Fig. S11 The magnetic coupling model of Gd(III) ions in cluster 4. ....	S7
Fig. S12 Temperature dependence of the ac magnetic susceptibility for 5.....	S8

<sup>a</sup> Department of Chemistry, Taiyuan Normal University, Jinzhong 030619, China.

<sup>b</sup> Department of Chemistry, Tianjin University, Tianjin, 300072, China.

\*Corresponding Authors E-mail : [cuijianzhong@tju.edu.cn](mailto:cuijianzhong@tju.edu.cn), [wuzhilei03@163.com](mailto:wuzhilei03@163.com)

Fig. S13 Frequency dependence of  $\chi'$  and  $\chi''$  for 6 at 2.0–16.0 K under a 0 dc field.

.....S8

## Experimental section

### Instrumentation

Elemental analyses (EA) for C, H, and N were performed on a Perkin-Elmer 240 CHN elemental analyzer. IR spectra were recorded in KBr pellets during the range of 4000–650  $\text{cm}^{-1}$  with a Bruker TENOR 27 spectrophotometer. PXRD data were examined on a Rigaku Ultima IV instrument with Cu  $K\alpha$  radiation ( $\lambda = 1.54056 \text{ \AA}$ ), with a scan speed of  $5^\circ \text{ min}^{-1}$  in the range of  $2\theta = 5\text{--}50^\circ$ . TGA measurements were obtained in an air atmosphere on a Labsys NETZSCH TG 209 Setaram apparatus from 40 to 800  $^\circ\text{C}$  with a heating rate of  $10^\circ \text{C min}^{-1}$ . UV–vis spectra were measured with a JASCO V-570 spectrophotometer at room temperature. Luminescence properties were recorded on an F-4500 FL spectrophotometer with a xenon arc lamp as the light source. The magnetic measurements were carried out with a Quantum Design MPMS-XL7 and a PPMS-9 ACMS magnetometer. The diamagnetic corrections for the complexes were estimated using Pascal's constants, and magnetic data were corrected for diamagnetic contributions of the sample holder.

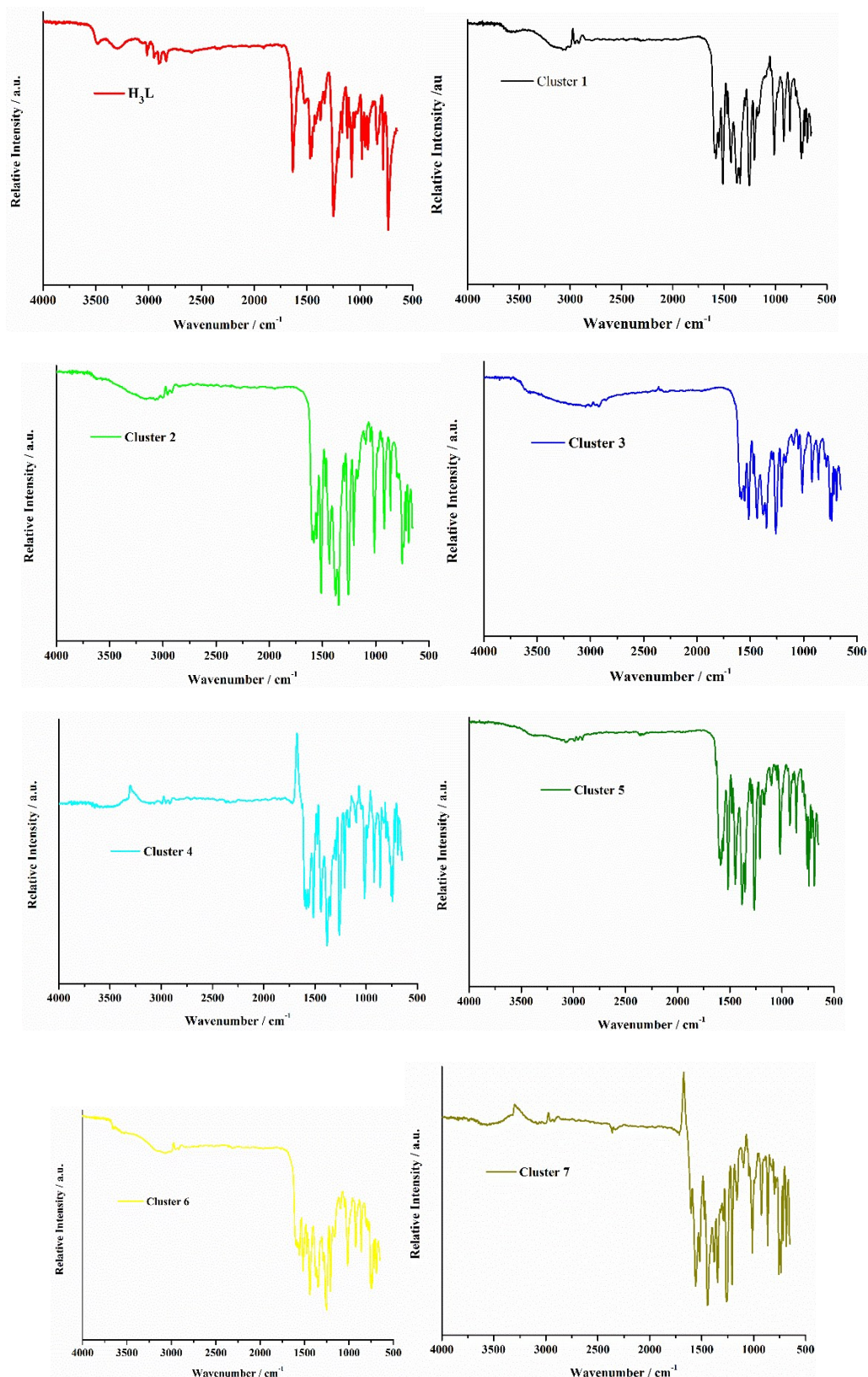
Table S1 The  $\text{Ln}^{\text{III}}$  geometry analysis by SHAPE 2.0 for clusters 6 and 7.

Cluster 6	$C_{4v}$ JCSAPR	$C_{4v}$ CSAPR	$D_{3h}$ JTCTPR	$D_{3h}$ TCTPR	$C_s$ MFF
Dy1 <sup>III</sup>	1.892	0.683	2.592	0.800	0.924
	$D_{4d}$ SAPR	$D_{2d}$ TDD	$C_{2v}$ JBTPR	$C_{2v}$ BTPR	$D_{2d}$ JSD
Dy2 <sup>III</sup>	1.735	0.900	2.049	1.866	2.880
Cluster 7	$D_{4d}$ SAPR	$D_{2d}$ TDD	$C_{2v}$ JBTPR	$C_{2v}$ BTPR	$D_{2d}$ JSD
Er1 <sup>III</sup>	2.635	2.066	2.493	1.542	4.710
Er2 <sup>III</sup>	3.893	2.435	3.123	2.272	3.977
	$D_{5h}$ PBPY	$C_{3v}$ COC	$C_{2v}$ CTPR	$D_{5h}$ JPBPY	
Er3 <sup>III</sup>	2.184	4.845	3.696	5.529	

SAPR-8 = Square antiprism; TDD-8 = Triangular dodecahedron; JBTPR-8 = Biaugmented trigonal prism J50; BTPR-8 = Biaugmented trigonal prism; JSD-8 = Snub diphenoid J84.

JCSAPR-9 = Capped square antiprism J10; CSAPR-9 = Spherical capped square antiprism; JTCTPR-9 = Tricapped trigonal prism J51; TCTPR-9 = Spherical tricapped trigonal prism; MFF-9 = Muffin.

PBPY-7 = Pentagonal bipyramid; COC-7= Capped octahedron; CTPR-7 = Capped trigonal prism; JPBPY-7 = Johnson pentagonal bipyramid J13.



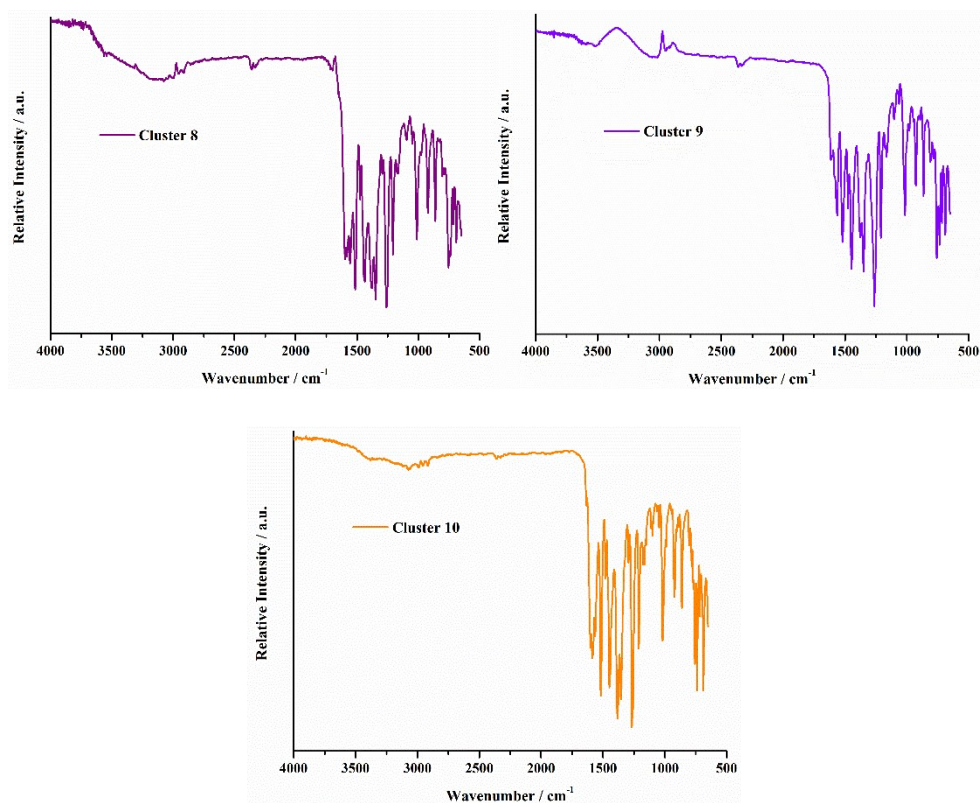


Fig. S1 The IR spectra of H<sub>2</sub>L ligand and clusters 1-10.

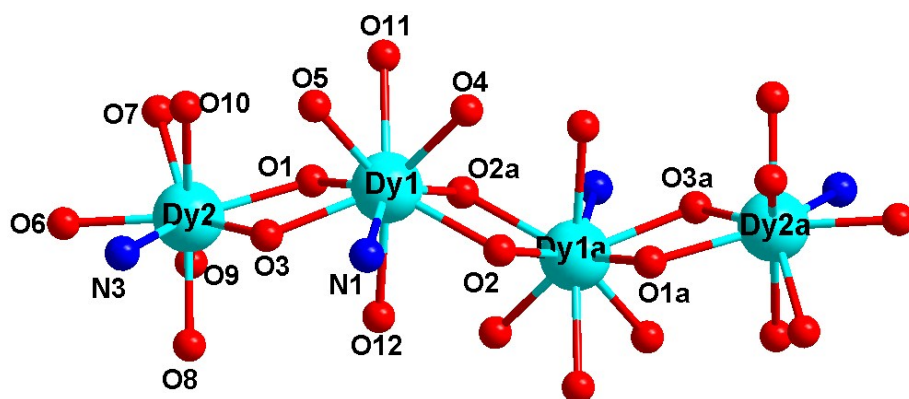


Fig. S2 The coordinate atom labels of central Dy(III) ions in cluster 6.

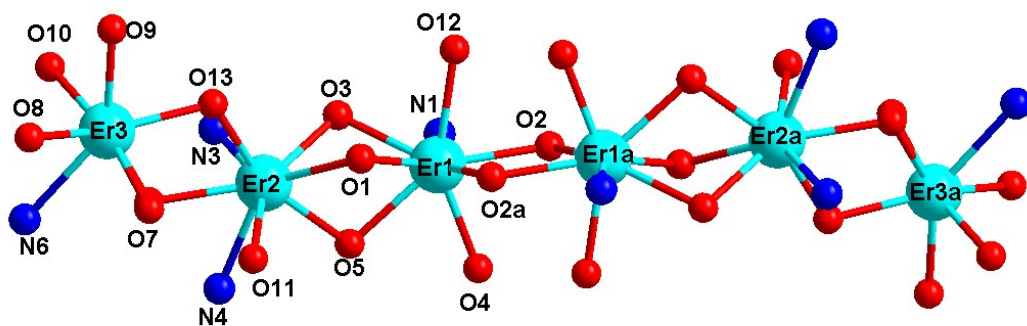


Fig. S3 The coordinate atom labels of central Er(III) ions in cluster 7.

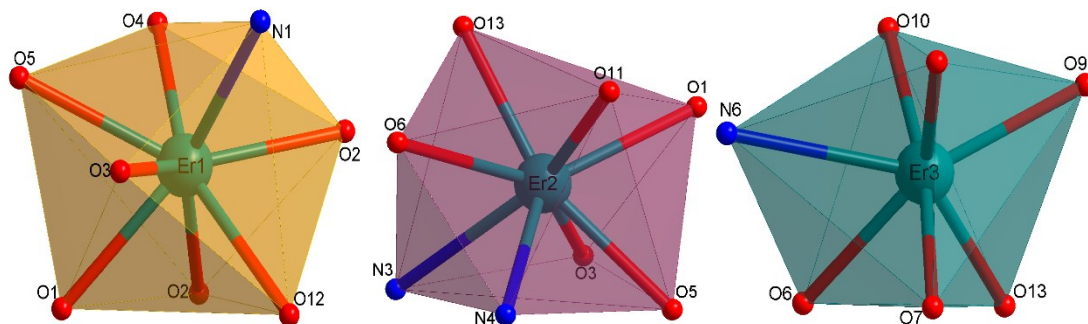


Fig. S4 Coordination polyhedra for Er1, Er2 and Er3 ions observed in cluster 7.

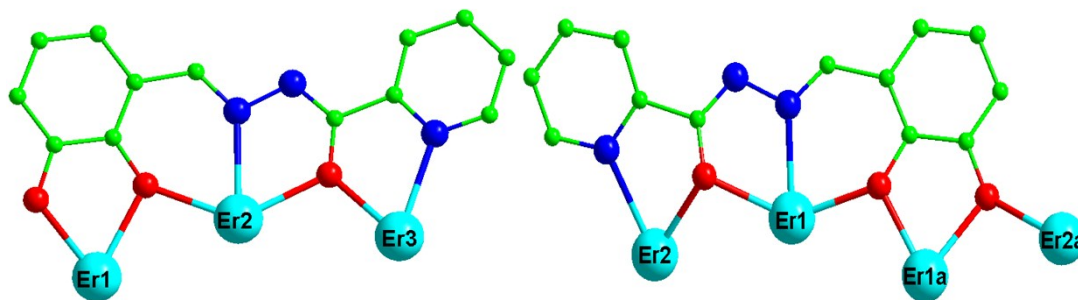


Fig. S5 Coordination modes of H<sub>2</sub>L in 7 (green, C; red, O; blue, N; and turquoise, Er).

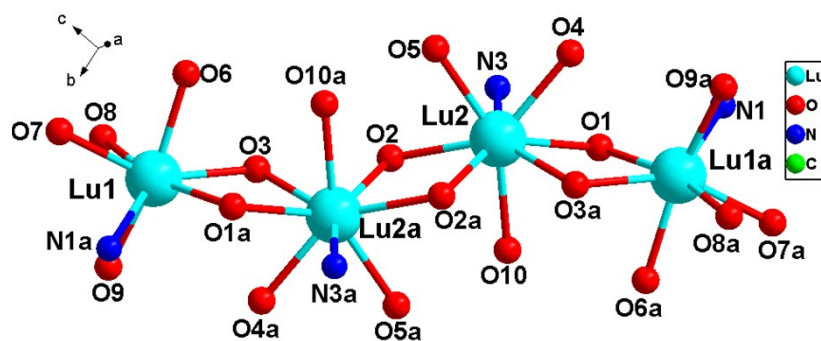


Fig. S6 The coordinate atom labels of central Lu(III) ions in cluster 10.

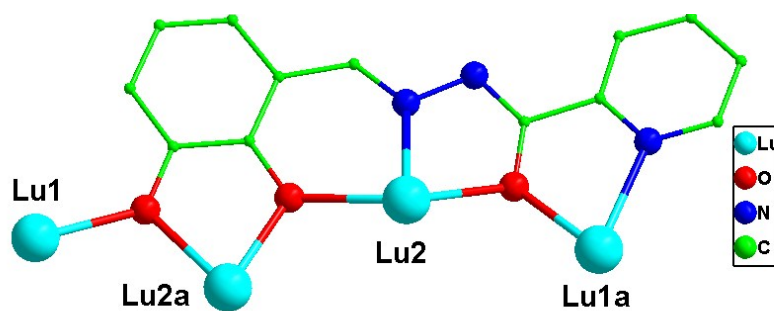
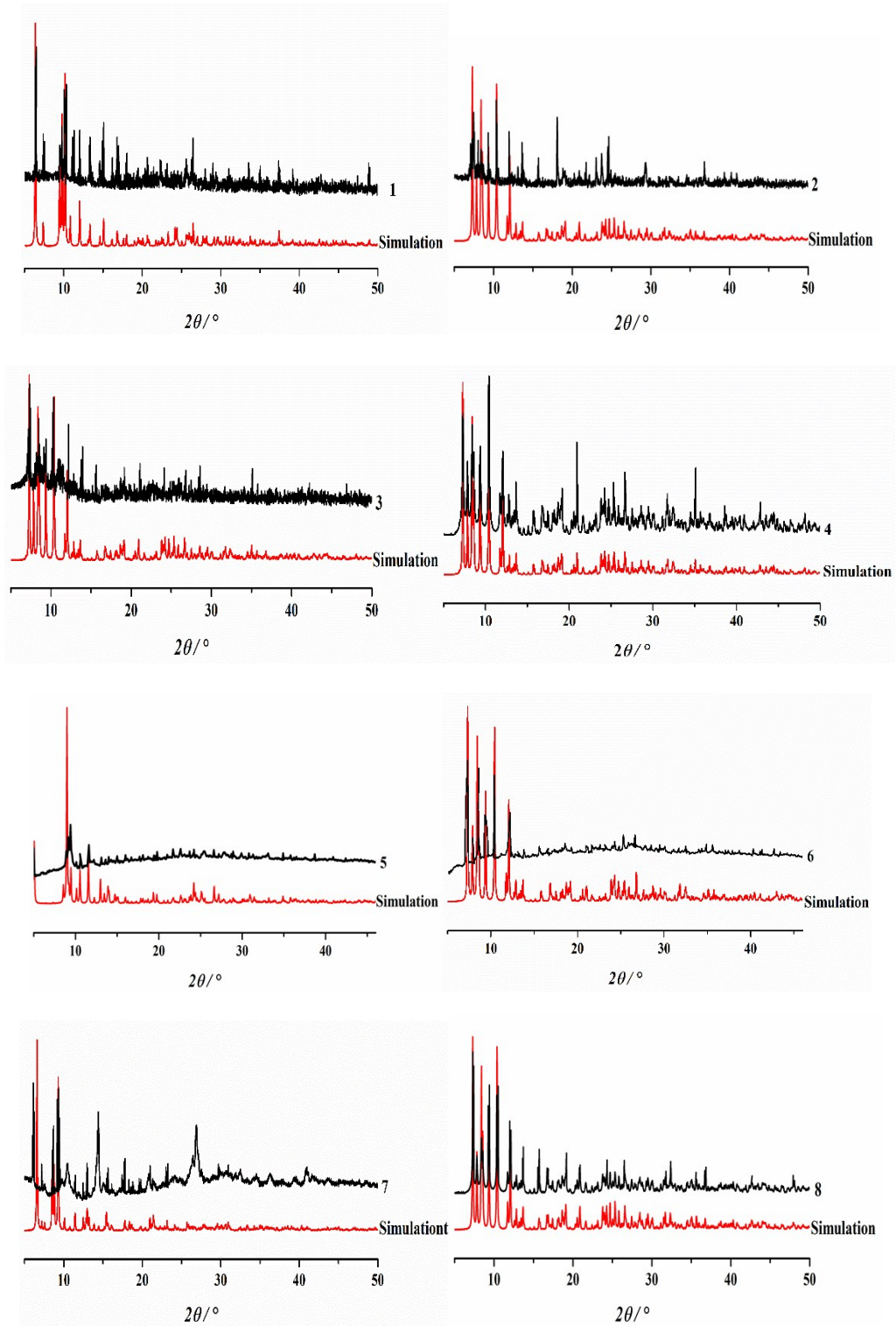


Fig. S7 Coordination modes of H<sub>2</sub>L in cluster 10.



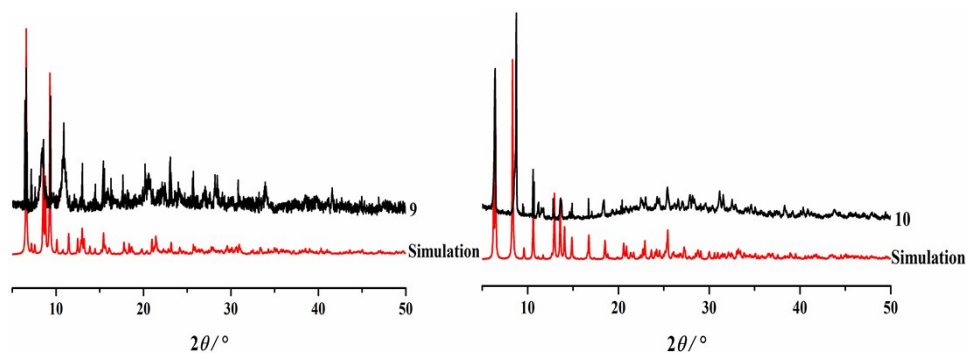


Fig. S8 PXRD patterns for clusters 1-10.

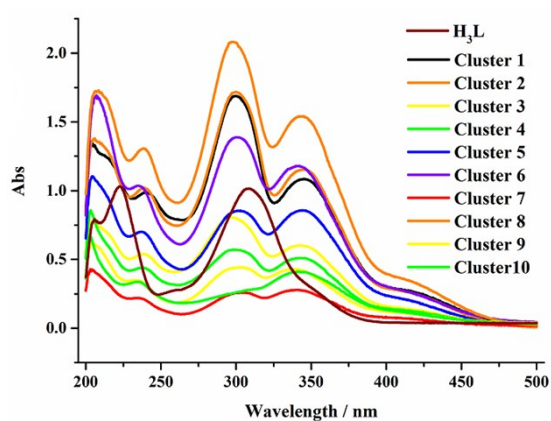


Fig. S9 The UV-vis spectra of clusters 1-10 and the  $H_3L$  ligand were performed at room temperature in ethanol solution.

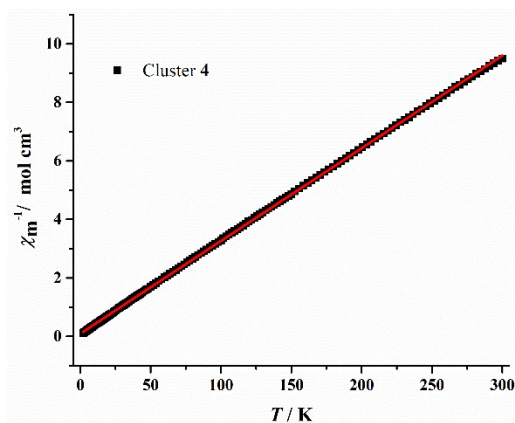


Fig. S10 Plots of  $\chi_M^{-1}$  vs  $T$  for cluster 4. The solid line was generated from the best fit by the Curie-Weiss expression.



Fig. S11 The magnetic coupling model of Gd(III) ions in cluster 4.

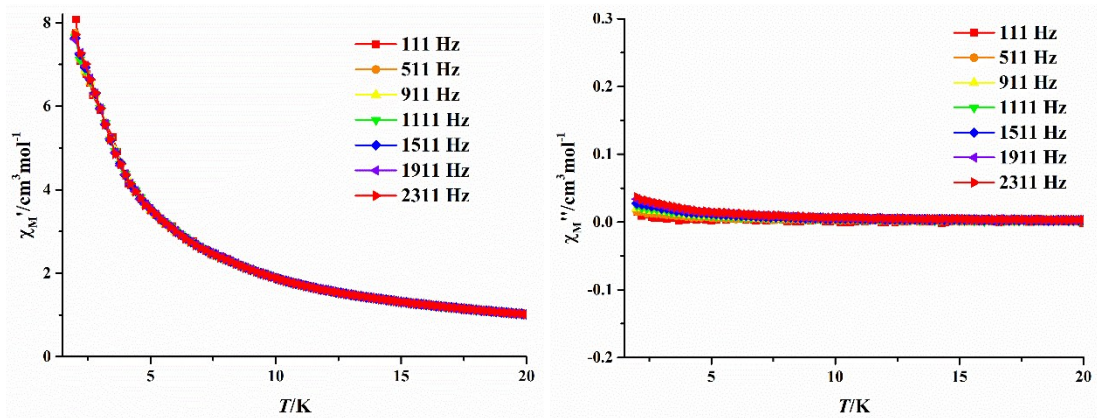


Fig. S12 Temperature dependence of the in-phase (left) and out-of-phase (right) components of the ac magnetic susceptibility for 5 in zero dc field with an oscillation of 3.0 Oe.

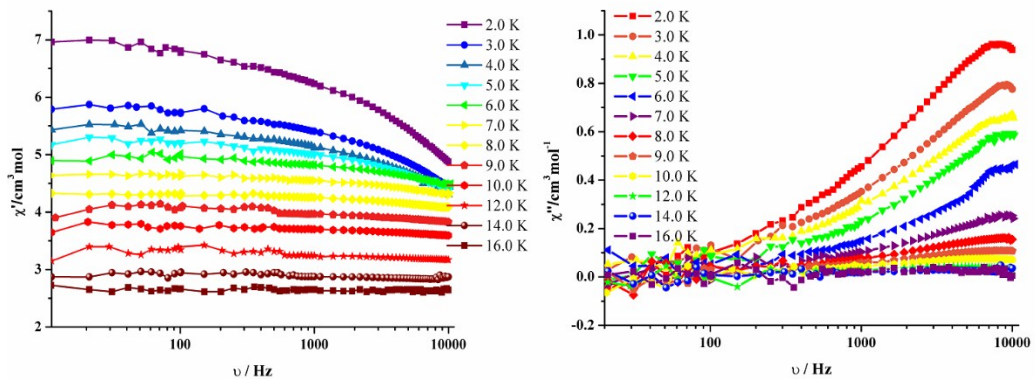


Fig. S13 Frequency dependence of  $\chi'$  and  $\chi''$  for 6 at 2.0–16.0 K under a 0 dc field.